Available online at www.sciencedirect.com
ScienceDirect
International Journal of Heat and Mass Transfer 51 (2008) 672–682
International Journal of HEAT and MASS TRANSFER
www.elsevier.com/locate/ijhmt

A numerical study of solidification in powder injection molding process

Sudip K. Samanta [a], Himadri Chattopadhyay [a,*], Björn Pustal [b], Ralf Berger [b], Mahadev Malhar Godkhindi [c], Andreas Bührig-Polaczek [b]

[a] Central Mechanical Engineering Research Institute, Durgapur 713 209, India
[b] Foundry Institute, RWTH Aachen, 52072 Aachen, Germany
[c] Department of Metallurgical and Materials Engineering, Indian Institute of Technology, Kharagpur 721 302, India

Received 28 April 2006; received in revised form 13 April 2007
Available online 3 July 2007

Abstract

Thermal analysis of mold filling and post-filing solidification has been carried out for the powder injection molding process. The filling material comprised alumina powder and polymeric binder was used to fill a rectangular cavity. The interphase momentum transfer was accounted for using a momentum exchange model due to Wang et al. [Y. Wang, S. Ahuja, C.Beckerman, H.C. de GROH III, Multi-particle interfacial drag in equiaxed solidification, Metall. Mater. Trans. B 26B (1995) 111–119]. Though both the alumina powder and polymeric binder are treated as fluids, as the alumina powder does not undergo a phase change, only the solidification of the binder has to be considered. The liquid fraction of the binder was assumed to follow a linear rule between the liquidus and solidus temperature. An iterative latent heat recovery formulation has been developed to obtain the liquid fraction during solidification. It was found that the predictions for pressure rise at the inlet compares favorably with the results from the single-phase mixture model. However, the multi-phase model could predict the powder segregation unlike the mixture model. The multi-phase model predicts higher temperature compared to mixture model due to powder particle migration.

Keywords: Powder injection molding; Solidification; Heat transfer; Simulation

1. Introduction

The powder injection molding (PIM) process is relatively one of the new near net shape manufacturing processes to produce metallic/ceramic small and complex engineering components in large quantities. PIM consists of four stages *viz.* feedstock preparation, injection stage, debinding stage and sintering stage. Thermoplastic polymer, which is also called binder is melted and mixed with powder (metal or ceramic) to form a feedstock (feedstock preparation) that can be injection molded (injection stage). After shaping the polymer, binder is extracted (in the debinding stage) and the powder is sintered (at the sintering stage), often to near theoretical densities. Among all the stages, the injection stage is most critical since defects like sink marks, voids, weld line, short shot and powder-binder segregation occurs in this stage due to improper specification of injection stage parameters and these defects cannot be repaired in the debinding or the sintering stage [1–3]. Injection stage parameters include injection pressure, injection temperature, mold temperature, post filling solidification time and mold design. The injection stage includes both the mold filling process and the post-filling solidification. These defects can be rectified by optimizing process parameters and mold design with trial and error technique. But this technique is time consuming and costs dearly. To avoid trial and error technique an insight into the injection stage is important for parameters optimization and science based mold design.

Till date few research works have been reported [4–14] to numerically analyze the injection stage of PIM and there is hardly any commercial package available to describe this

* Corresponding author.
E-mail address: chimadri@gmail.com (H. Chattopadhyay).

0017-9310/$ - see front matter © 2007 Elsevier Ltd. All rights reserved.
doi:10.1016/j.ijheatmasstransfer.2007.04.033

Nomenclature

C_D	drag coefficient
d_a	particle size of air, m
$C_p(\phi_e)$	particle shape factor
$f_{s,max}$	maximum solids loading
g	gravity acceleration, m s^{-2}
H	heat transfer coefficient, W m^{-2} K^{-1}
K	momentum exchange coefficient, kg m^{-3} s^{-1}
Nu	Nusselt number
Pr	Prandlt number
Re	Reynolds number
T	temperature, K
T_0	reference temperature for density definition, K
T^s	solidus temperature of binder, K
$\mathbf{U}$	momentum exchange due to drag force, kg m^{-2} s^{-2}
μ	viscosity, kg m^{-1} s^{-1}
c_p	specific heat, J kg^{-1} K^{-1}
d_s	powder particle diameter, m
f	volume fraction
F	fraction of liquid
h	enthalpy, J kg^{-1}
k	thermal conductivity, W m^{-1} K^{-1}
L	latent heat, J/kg
P	pressure, Pa
Q	energy exchange by heat transfer, J m^{-3} s^{-1}
t	time, s
T^l	liquidus temperature of binder, K
T_{ref}	reference temperature for enthalpy definition, K
$\vec{\mathbf{u}}$	velocity vector, m s^{-1}
ρ	density, kg m^{-3}
$\bar{\bar{\tau}}$	stress–strain tensors, kg m^{-1} s^{-2}

Subscripts

l, s, a, m stands for binder, powder, air and powder-binder mixture phases, respectively

Abbreviation

1-p single-phase
2-p multi-phase

injection stage in PIM. The literature review shows that researchers have addressed mainly the flow pattern during the mold filling process of the injection stage. To simulate the mold filling process majority of the researchers [4–10] have considered feedstock melt as a homogeneous single fluid with properties of the mixture and single set of conservation equation is solved to simulate the mold filling. On the other hand, in a relatively new approach, multiphase flow concepts have been applied by some of the researchers [11–14] to take care of the heterogeneous behavior of the feedstock. In this approach, it is considered that the feedstock melt is composed of two separate fluids: powder and binder, where powder is considered as one fluid with its own properties and binder is another fluid with its own properties. Two separate sets of conservation equations are solved simultaneously and an interaction term is introduced for momentum transfer between the phases. Also it may be noted that researchers [12–14] who have employed the multiphase approach, did not carry out non-isothermal simulation, which resembles the actual filling process. They also did not take into account the non-Newtonian rheological behaviour of the phases and used constant value for the phase interaction coefficient which really depends on the viscosity of the primary phase and the volume fraction of the secondary phase. Literature review shows that none of the researchers have taken care of the solidification issue during mold filling and post filling where semi-crystalline polymer solidifies releasing latent heat. Solidification dictates mold design issue, that is, critical thickness of the mold cavity can be determined if solidification pattern and time is known. Also defects like weld lines can be avoided in the injected component if solidification pattern and time is known.

In view of the above, in the present investigation, simulation of the injection stage of PIM has been developed with a multiphase flow approach to address the solidification issue during mold filling and post filling. It may be mentioned here that the prediction of segregation in single-phase modeling requires the prescription of the relative velocity between individual phases. Multiphase flow approach has been chosen since it can predict phase separation and due to phase separation effect temperature profile inside the mold may be different [11] because of change of overall thermal properties which in turn affects solidification of feedstock. This phenomenon of phase separation is very important since slight change in feedstock composition produces strong anisotropy in the final product [5].

2. Statement of the problem

A rectangular mold cavity as shown in Fig. 1 has been selected to simulate the filling process of PIM. It is assumed that mold wall thickness is 20 mm and after the mold wall thickness of 20 mm, water is circulating to control the mold temperature. The molten feedstock temperature at the inlet is 500 K and circulating water temperature is 343 K. For simulation purposes, it is assumed that powder volume fraction and binder volume fraction is uniform at inlet and fed at a uniform velocity. Non-isothermal simulation with feedstock as single phase and with feedstock as two separate phases (powder and binder) are carried out. It is assumed that the mold is filled with constant velocity at the left side

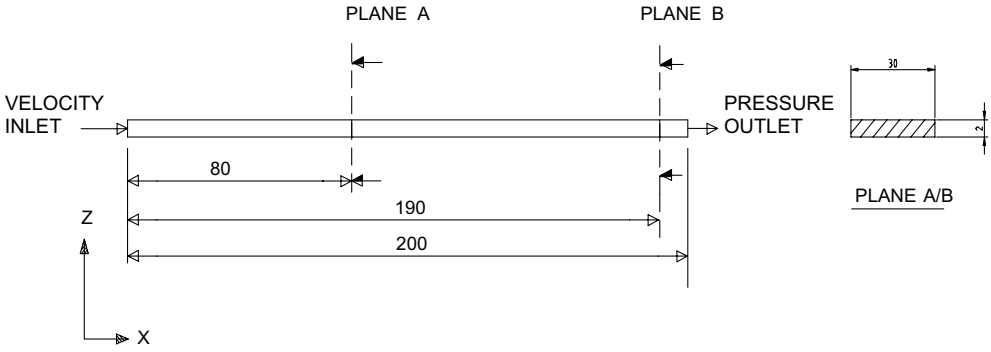

Fig. 1. Computational domain.

inlet. The right side of the mold is exposed to atmospheric condition. From simulation with feedstock as two phase, segregation of powder and binder is directly predicted and injection pressure developed at inlet and temperature during mold filling and solidification are compared with the results simulated with feedstock as single phase.

2.1. Material model

In the present work, the filling material is composed of 37 vol.% alumina powder of 5 μm diameter and 63 vol.% binder (LDPE, PE wax and stearic acid together) [8]. Table 1 shows the thermal and rheological properties of the materials involved in the present study.

Since latent heat data and binder liquidus (upper crystallization) temperature and solidus(lower crystallization) temperature are not available, the data of low density polyethylene are used. So, the solidus temperature is 348 K, the liquidus temperature is 393 K and latent heat of binder is taken as 130 kJ/kg. Latent heat of feedstock is determined by mixture rule considering latent heat of powder is zero since it does not melt and solidify.

$$L_m = f_l L_l$$

Thermal conductivity and specific heat of powder, which are not readily available, are again determined by applying mixture rule.

$$C_{p(m)} = f_s C_{p(s)} + f_l C_{p(l)}$$

Table 1
Thermal properties of feedstock and binder and rheological parameters (cross model) [8]

	Feedstock	Binder
Density, ρ [kg/m^3]	2.09×10^3	1.0×10^3
Specific HEAT, C_p [J/(kg K)]	6.78×10^2	2.26×10^2
Thermal conductivity, k [W/(mK)]	8.73	0.74
Latent heat [L(J/kg)]	81,900	130,000
Power law index [n]	0.3283	0.4221
T_b [K]	5.683×10^3	4.881×10^3
B [kg/(m s)]	9.539×10^{-3}	1.561×10^{-2}
C [kg/(m s^2)$^{n-1}$]	4.648×10^{-4}	3.293×10^{-3}

From the previous works [1–3,5], it is well known that powder binder mixture as well as the binder behaves like shear thinning fluid which is required for successful PIM mold filling. Neglecting the pressure effect on viscosity (since it is small compared to shear rate and temperature dependency) powder binder mixture and binder viscosity is defined by Non-Newtonian Cross model (Eq. (1)), which describes shear rate and temperature dependence of viscosity.

$$\eta(\gamma, T) = \frac{\eta_0}{1 + c(\eta_0 \gamma)^{1-n}}, \tag{1}$$

where,

$$\eta_0 = B \cdot \exp(T_b/T) \tag{2}$$

The mixture or the feedstock as well as the binder alone was characterized by Kown et al. [8]. The values are straight adopted from this source and reproduced in Table 1.

In order to determine the viscosity of powder, first the mixture viscosity model due to Ishii et al. [15] was used to determine the combined viscosity.

$$\mu_m = \mu_l \left(1 - \frac{f_s}{f_{s,\max}}\right)^{-2.5 f_{s,\max}} \tag{3}$$

Now the powder viscosity can be obtained using the following mixture rule:

$$\mu_s = \frac{\mu_l}{f_s}\left(\left(1 - \frac{f_s}{f_{s,\max}}\right)^{-2.5 f_{s,\max}} - (1 - f_s)\right) \tag{4}$$

To model solidification of binder and mixture it is assumed that there is no flow and hence the viscosity of binder and mixture is increased to a very high value below the solidus or lower crystallization temperature of binder.

3. Mathematical formulation

3.1. Governing equations

Since the binder volume fraction is considerably higher, the binder is treated as the primary fluid. Alumina powder was considered as the secondary phase. In addition to the two phases present, it is essential to consider the presence of the third phase which is air. This air is present inside

the mold before powder and binder mixture fills the mold replacing the air.

For each phase, a separate set of continuity, momentum and energy equations are solved but same pressure field is shared by all the phases. A momentum exchange term and heat exchange term are included in the transport equations to take care of momentum and heat transfer between the phases.

The governing equations are:

A. *Continuity*:

$$\frac{\partial}{\partial t}(f_p\rho_p) + \nabla\cdot(f_p\rho_p\vec{\mathbf{u}}_p) = 0, \tag{5}$$

where p denotes an individual phase, $p \in$ (s, l, a)

$$f_\mathrm{l} + f_\mathrm{s} + f_\mathrm{a} = 1 \tag{6}$$

B. *Momentum*:

$$\frac{\partial}{\partial t}(f_\mathrm{l}\rho_p\vec{\mathbf{u}}_p) + \nabla\cdot(f_p\rho_p\vec{\mathbf{u}}_p\vec{\mathbf{u}}_p) = -f_\mathrm{l}\nabla p + \nabla\cdot\bar{\bar{\tau}}_\mathrm{l} + f_l\rho_p\mathbf{g} + \mathbf{U}_{pij}, \tag{7}$$

where $\overline{\overline{\tau_p}} = \mu_p f_p(\nabla\vec{\mathbf{u}}_p + (\nabla\vec{\mathbf{u}}_p)^T)$.

Phase interactions (e.g. drag and friction) for a liquid–solid mixture

$$\mathbf{U}_\mathrm{ls} = -\mathbf{U}_\mathrm{sl}$$

$$\mathbf{U}_\mathrm{ls} = K_\mathrm{ls}(\mathbf{u}_\mathrm{l} - \mathbf{u}_\mathrm{s}) \tag{8}$$

$$\mathbf{U}_\mathrm{as} = -\mathbf{U}_\mathrm{sa} = K_\mathrm{as}(\vec{\mathbf{u}}_\mathrm{s} - \vec{\mathbf{u}}_\mathrm{a}) \tag{9}$$

$$\mathbf{U}_\mathrm{la} = -\mathbf{U}_\mathrm{al} = K_\mathrm{la}(\vec{\mathbf{u}}_\mathrm{l} - \vec{\mathbf{u}}_\mathrm{a}) \tag{10}$$

The drag force coefficient, K_ls and K_sa, is calculated by employing the model developed by Wang et al. [16].

$$K_\mathrm{ls} = \frac{4\beta^2\mu_\mathrm{l}}{d_\mathrm{s}^2}f_\mathrm{l}^2, \tag{11}$$

where

$$\beta = \left[\frac{9}{2}(1-f_\mathrm{l})\frac{2+\frac{4}{3}\eta^5}{2-3\eta+3\eta^5-2\eta^6}\frac{1}{C_p(\phi_\mathrm{e})}\right]^{1/2}$$

with

$$\eta = (1-f_l)^{1/3}$$

$$C_p(\phi_\mathrm{e}) = \phi_\mathrm{e}^2 \quad 0.0 < f_\mathrm{l} < 0.7$$

$$C_p(\phi_\mathrm{e}) = 1.26\log_{10}\left(\frac{\phi_\mathrm{e}}{0.163}\right) \quad 0.7 < f_\mathrm{l} < 1.0$$

K_as can be calculated in an analogus manner.

For liquid–air, the source terms are calculated by

$$\mathbf{U}_\mathrm{la} = -\mathbf{U}_\mathrm{al} = \mathbf{U}_\mathrm{la} = K_\mathrm{la}(\vec{\mathbf{u}}_\mathrm{l} - \vec{\mathbf{u}}_\mathrm{a}) \tag{12}$$

Schiller and Naumann's model [17] is used for calculating K_la.

$$K_\mathrm{la} = 3\mu_\mathrm{l}f_\mathrm{l}f_\mathrm{a}C_\mathrm{D}Re/(4d_\mathrm{a}^2), \tag{13}$$

where d_a is the characteristic diameter of air which is used for calculating drag force only. C_D is drag coefficient that is based on the relative Reynolds number Re. It may be mentioned here that the model requires the characteristics diameter of gaseous phase, which may be interpreted as the average space occupied by air phase surrounded by the binder and powder phases. The prescribed diameter of air is indeed very small at 5 μm.

$$C_\mathrm{D} = \begin{cases} 24(1+0.15Re^{0.687})/Re & Re \leqslant 1000 \\ 0.44 & Re > 1000 \end{cases} \tag{14}$$

with $Re = \frac{\rho_\mathrm{l}|\vec{\mathbf{u}}_\mathrm{a} - \vec{\mathbf{u}}_\mathrm{l}|d_\mathrm{a}}{\mu_\mathrm{l}}$.

C. *Energy*:

$$\frac{\partial}{\partial t}(f_P\rho_P h_P) + \nabla\cdot(f_p\rho_p\vec{\mathbf{u}}_p hp) = -f\frac{\partial p}{\partial t} + \bar{\bar{\tau}} : \nabla\vec{\mathbf{u}}_p + \nabla\cdot(f_p k_p\nabla T_p), \tag{15}$$

where $h_\mathrm{l} = \int_{T_\mathrm{ref}}^{T_l} c_{p(l)}\mathrm{d}T + h_\mathrm{l}^\mathrm{ref}$ The source terms of enthalpy transfer for liquid/air is calculated by

$$Q_\mathrm{la} = -Q_\mathrm{al} = H_\mathrm{la}\cdot(T_\mathrm{l} - T_\mathrm{a}) \tag{16}$$

The heat exchange coefficient, H_la is calculated as

$$H_\mathrm{la} = 6k_\mathrm{l}f_\mathrm{l}f_\mathrm{a}Nu_\mathrm{a}/d_\mathrm{a}^2, \tag{17}$$

where Nu_a is the Nusselt number calculated by Ranz et al. model [18] as follows:

$$Nu_\mathrm{a} = 2.0 + 0.6Re_\mathrm{a}^{1/2}Pr^{1/3}, \tag{18}$$

where

$$Pr = \frac{C_{p(l)}\mu_\mathrm{l}}{k_\mathrm{l}} \tag{19}$$

On the other hand, the source terms of enthalpy transfer for binder/powder is calculated by

$$Q_\mathrm{ls} = -Q_\mathrm{sl} = H_\mathrm{ls}\cdot(T_\mathrm{l} - T_\mathrm{s}) \tag{20}$$

The heat exchange coefficient, H_ls is calculated as

$$H_\mathrm{ls} = 6k_\mathrm{l}f_\mathrm{l}f_\mathrm{s}Nu_\mathrm{s}/d_\mathrm{s}^2, \tag{21}$$

where Nu_s is the Nusselt number calculated by Gun model [19] as follows:

$$Nu_\mathrm{s} = (7 - 10f_\mathrm{l} + 5f_\mathrm{l}^2)(1 + 0.7Re_\mathrm{s}^{0.2}Pr^{1/3}) + (1.33 - 2.4f_\mathrm{l} + 1.2f_\mathrm{l}^2)Re_\mathrm{l}^{0.7}Pr^{1/3} \tag{22}$$

For air and powder, source term for enthalpy transfer is calculated by,

$$Q_\mathrm{as} = -Q_\mathrm{sa} = H_\mathrm{as}\cdot(T_\mathrm{a} - T_\mathrm{s}) \tag{23}$$

The heat exchange coefficient, H_ls is calculated as

$$H_\mathrm{asa} = 6k_\mathrm{a}f_\mathrm{a}f_\mathrm{s}Nu_\mathrm{s}/d_\mathrm{s}^2, \tag{24}$$

where Nu_s is the Nusselt number calculated by Gun model [19] as follows:

$$Nu_\mathrm{s} = (7 - 10f_\mathrm{a} + 5f_\mathrm{a}^2)(1 + 0.7Re_\mathrm{s}^{0.2}Pr^{1/3}) + (1.33 - 2.4f_\mathrm{a} + 1.2f_\mathrm{a}^2)Re_\mathrm{s}^{0.7}Pr^{1/3}, \tag{25}$$

where

$$Pr = \frac{C_{p(a)}\mu_\mathrm{a}}{k_\mathrm{a}} \tag{26}$$

3.2. Solidification model

It is already mentioned that both the metallic powder and polymeric binder are treated as fluid in the present multiphase model. However, solidification of the mixture is only involves the phase change of the binder. Based on the liquid fraction of binder and latent heat of the binder (since most of the binder are semi crystalline as binder is a blend of various polymers and waxes), temperature of the binder is modified continuously by temperature recovery method in the range of temperature, where binder is being solidified that is at temperatures where crystallization of the binder starts (liquidus temperature) and where total crystallization is finished (solidus temperature) i.e. where binder becomes solid. It must be mentioned here that binder melts and solidify but powder does not melt and solidify. Though the solidification curve of semi-crystalline polymer binder is essentially non-linear, assuming linearity of the curve does not make significant deviation in liquid fraction as established in literature [20].

The liquid fraction is calculated by solving a scalar transport Eq. (27) with zero mass flow rate and zero diffusion flux since there is no mass transfer and no diffusion.

$$\frac{\partial}{\partial t}(\rho_l F_l) + \nabla \cdot (\rho_l F_l \vec{\mathbf{u}}_l) = 0 \tag{27}$$

Fig. 2 shows a schematic diagram of temperature fraction of liquid of binder. The line DCBA represents the line which binder should follow when binder solidifies with release of latent heat.

From Fig. 2, we get the slope of the line BC,

$$\frac{dF_l}{dT} = \frac{CP}{BP} = \frac{LM}{MN} = \frac{1}{T^l - T^s} \tag{28}$$

Also, from conservation of energy in the mushy region, we can write that,

$$L_l dF_l + C_{pl} dT = 0 \tag{29}$$

so,

$$\frac{dF_l}{dT} = -\frac{C_{pl}}{L_l} \tag{30}$$

which represents the slope of the line EGKJF. The slope is negative because it states that as liquid fraction decreases, it releases more heat, so that as liquid fraction decreases temperature increases.

Now as temperature falls below liquidus temperature T^l and stays above T^s, by solving energy equation solver will give temperature and fraction of liquid at any point say e.g. at Point G. But we want solidification curve should follow the line CB. So, we must tell solver to follow this DCBA line. So, to follow this line, when solver gives us temperature as in point G, at that instant the actual temperature should be T_1 and it is given by

$$T_1 = T^s + (T^l - T^s) dF_l \tag{31}$$

As we change the temperature, fraction of liquid will change by following line EGKJF and Eq. (30) and we will land in the point J. However, to stay on line CB, the temperature has to be corrected leading to point K which is on line CB at any instant when temperature is between T^l and T^s.

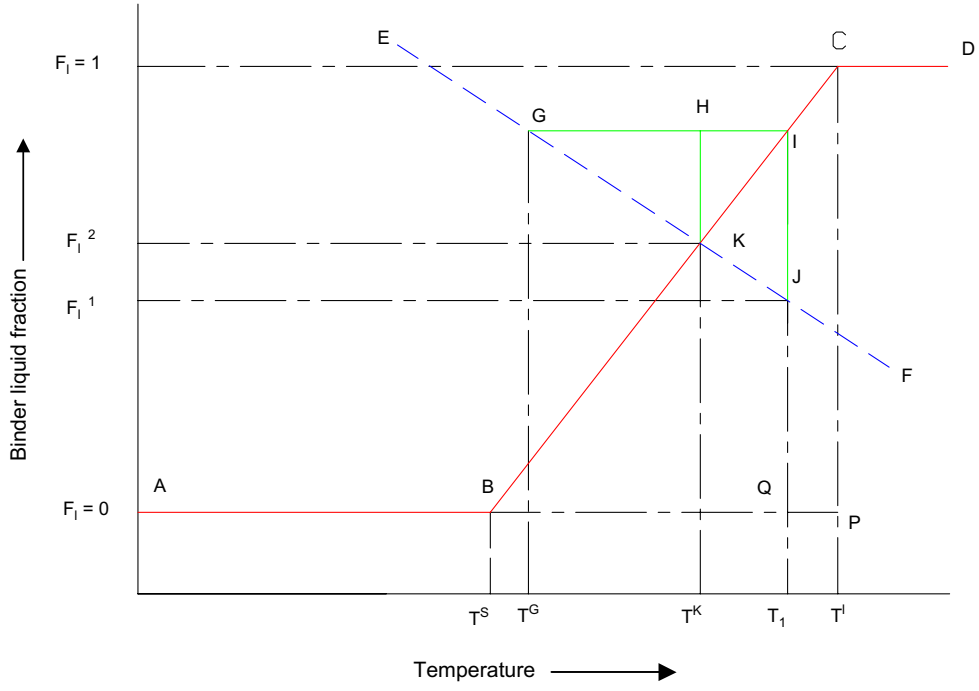

Fig. 2. Schematic diagram of temperature correction method.

From Eq. (28), we get,

$$\frac{\mathrm{KH}}{\mathrm{IH}} = \frac{\mathrm{d}F_\mathrm{l}}{\mathrm{d}T} = \frac{1}{T^\mathrm{l} - T^\mathrm{s}}$$

So,

$$\mathrm{IH} = \mathrm{d}T = \mathrm{KH}(T^\mathrm{l} - T^\mathrm{s}) = \mathrm{d}F_\mathrm{l}(T^\mathrm{l} - T^\mathrm{s}) \tag{32}$$

From Eq. (30) we get,

$$\mathrm{GH} = \mathrm{d}T = \mathrm{KH}\frac{L}{C_\mathrm{pl}} = \mathrm{d}F_\mathrm{l}\frac{L}{C_\mathrm{pl}} \tag{33}$$

From Eqs. (32) and (33) we get,

$$T_1 - T^\mathrm{G} = \mathrm{GI} = \mathrm{GH} + \mathrm{IH} = \mathrm{d}F_\mathrm{l}\frac{L}{C_\mathrm{pl}} + \mathrm{d}F_\mathrm{l}(T^\mathrm{l} - T^\mathrm{s})$$

or,

$$\mathrm{d}F_\mathrm{l} = \frac{T_1 - T^\mathrm{G}}{\frac{L_\mathrm{l}}{C_\mathrm{pl}} + (T^\mathrm{l} - T^\mathrm{s})} \tag{34}$$

So, we have corrected the fraction of liquid by Eq. (34) so that it lies in point K on line CB. Now, the we correct temperature so that it also lies on point K. If we change tem-

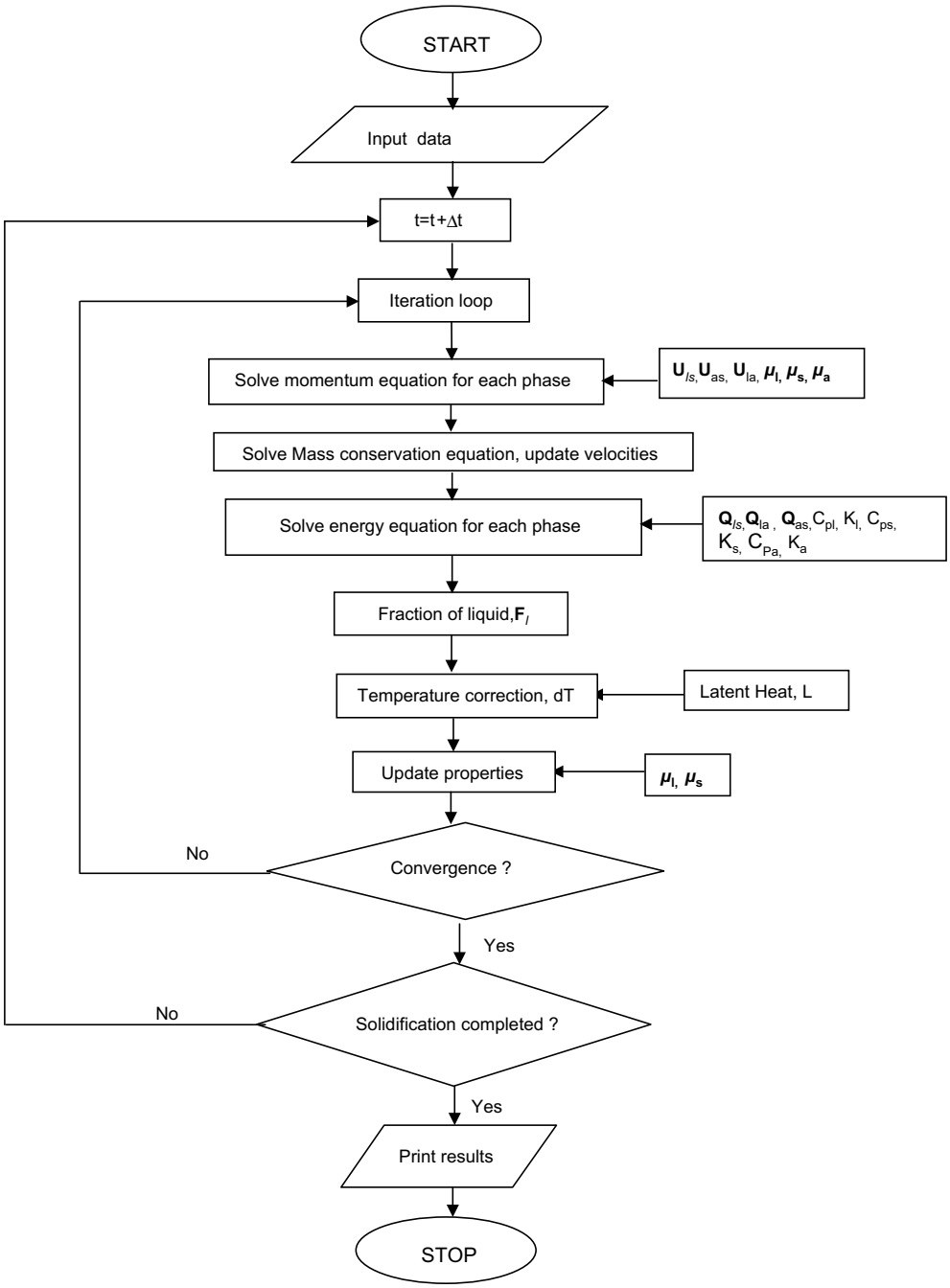

Fig. 3. Flow chart of the computational scheme.

perature from point G to point H that is an amount of GH we will reach on point K on line CB. From Eq. (30), we get,

$$\mathrm{GH} = \mathrm{d}T = \mathrm{d}F_\mathrm{l}\frac{L_\mathrm{l}}{C_\mathrm{pl}} \tag{35}$$

If we put the value of $\mathrm{d}F_\mathrm{l}$ from Eq. (34), the temperature correction is obtained which is to be added with temperature at point G (which solver initially gives us) to reach at point K.

$$\mathrm{d}T = \mathrm{d}F_\mathrm{l}\frac{L_\mathrm{l}}{C_\mathrm{pl}} = \frac{(T_1 - T^\mathrm{G})\frac{L_\mathrm{l}}{C_\mathrm{pl}}}{\frac{L_\mathrm{l}}{C_\mathrm{pl}} + (T^\mathrm{l} - T^\mathrm{s})} \tag{36}$$

So, the corrected temperature at Point K, T^K is,

$$T^\mathrm{K} = T^\mathrm{G} + \frac{(T_1 - T^\mathrm{G})\frac{L_\mathrm{l}}{C_\mathrm{pl}}}{\frac{L_\mathrm{l}}{C_\mathrm{pl}} + (T^\mathrm{l} - T^\mathrm{s})} \tag{37}$$

Once the solver returns the values of T and F_l, they are adjusted using the following relations:

$$\mathrm{d}F_\mathrm{l} = \frac{T_1 - T^\mathrm{G}}{\frac{L_\mathrm{l}}{C_\mathrm{pl}} + (T^\mathrm{l} - T^\mathrm{s})} \tag{38}$$

$$\mathrm{d}T = \mathrm{d}F_\mathrm{l}\frac{L_\mathrm{l}}{C_\mathrm{pl}} = \frac{(T_1 - T^\mathrm{G})\frac{L_\mathrm{l}}{C_\mathrm{pl}}}{\frac{L_\mathrm{l}}{C_\mathrm{pl}} + (T^\mathrm{l} - T^\mathrm{s})}. \tag{39}$$

3.3. Numerical procedure

The conservation equations reported in Section 3.1 are solved numerically by using a SIMPLE based control volume technique using the FLUENT(version 6.2) code as the solver-engine. The FLUENT code [21] has Eularian multiphase capability. However, the Wang model for phase interaction is not available there and the authors developed a C-based code [22]. Code was also developed for treating solidification in the manner described in Section 3.2. The flowchart of computation is presented in Fig. 3. FLUENT formulation is fully implicit and ideally there is no stability criteria to be met to define time step, Δt in transient problem for purely diffusion problems only. For the present situation, Δt is determined by numerical experiments and found that in this case $\Delta t = 0.001$ s gives optimum results. It is also found that for each time step 20 iterations are needed to reduce the normalized residuals below the convergence criteria of 10^{-5}. In each iteration, viscosity, momentum exchange, heat exchange, temperature and fraction of liquid (during solidification) correction are calculated by User Defined Functions (UDFs) written for the above. All the phases in the calculation domain shares a single pressure field solved by using phase coupled SIMPLE algorithm. The pressure correction equation is obtained from the sum of mass conservation equations (Eqs. (1)–(3)). The conservation equation of momentum, mass, energy and User Defined Scalar equation for Fraction of liquid are solved in the given order. Second order upwind scheme is used to discretize the momentum equation and first order upwind scheme is used for the rest of the equations. The dependent physical properties like viscosities are updated before staring of the next iteration. In the present model $\mathbf{u}_p$, f_p are coupled with each other via viscosity of the phases, momentum,heat exchange between the phases. The consequences of the coupling are that, for example, a change in momentum exchange model will affect the velocity field of the phases which will influence temperature and the temperature field in turn will affect the value of liquid fraction.

Table 2
Injection pressure and filling time

Sl. no.	Inlet temperature (K)	Wall temperature (K)	Injection pressure (MPa)	Filling time (s)
1	500	343	49.1(49.6)	2.823(2.803)
2	505	343	47.4(48.2)	2.828(2.795)
3	510	343	45.6(46.8)	2.814(2.788)
4	500	338	49.7(50.7)	2.844(2.811)
5	505	338	48.0(49.2)	2.822(2.804)
6	510	338	46.2(47.8)	2.827(2.792)
7	500	333	50.5(51.7)	2.839(2.814)
8	505	333	48.6(50.2)	2.82(2.804)
9	510	333	46.3(48.7)	2.815(2.802)

Bracketed terms indicate results of 1-p flow.

Regarding boundary condition, velocity inlet boundary condition is used at the inlet location where material is entering into the mold and pressure outlet boundary condition is used at the outlet for air vent as shown in Fig. 1. The usual no-slip condition is prescribed on the mold walls.

For computations using single-phase approach, the mixture is treated as a single fluid and properties of the mixture as shown in Table 2 (Feedstock column) measured in [8] have been used. The governing equations are similar to those for any phase of the multi-phase flow without the phase-interaction terms. Again, a similar solution strategy as reported for the multiphase flow was adopted.

4. Results and discussion

The computations were performed in a stretched grid of $30 \times 10 \times 10$. To achieve grid independence, several grid sizes were tried. As an example, Fig. 3 shows the development of pressure at the injection velocity of 0.1 m/s, at three different levels of grid. It can be seen that the coarser grid fails to show the developed pressure plateau while at the higher resolution, the results do not differ significantly. Thus a grid of 3000 cells was finally chosen.

Since no experimental data are available, the simulation results of feedstock as two phase flow and results of feedstock as single phase flow are compared. As such, single-phase models are quite capable in predicting bulk flow characteristics including injection pressure. Injection pressure required at inlet to maintain the constant flow rate is an important parameter to validate the simulation results because it can be measured directly from the injection

molding machine and there is a direct mathematical expression available [23] for cylindrical geometry to calculate injection pressure for constant flow rate in transient flow when Power Law model is used to describe the viscosity in isothermal case. Fig. 4 shows comparison between prediction of 2-p and 1-p injection pressure developed at inlet during mold filling. The prediction of 2-p pressure is very close to 1-p injection pressure. Table 2 shows how maximum injection pressure varies in order to maintain a constant velocity of 0.1 m/s. The table also indicates a comparison of 2-phase and 1-phase flow results. Referring back to Table 2, it can be observed that at a fixed mold temperature, as the inlet temperature increases, maximum injection pressure decreases in both 2-p as well as 1-p calculations. As such the results of 2-p and 1-p pressure prediction are very close. This is because as the temperature increases, if we look at the viscosity models of binder as well as powder, the viscosity decreases leading to reduced injection pressure developed while maintaining constant flow rate prescribed through velocity boundary condition. On the other hand, at fixed inlet temperature, as the mold temperature decreases the overall temperature inside the mold decreases due to faster heat release from the mold leading to higher viscosity and thereby, increased pressure. Also it can be seen that increasing or decreasing inlet temperature has more pronounced effect on maximum pressure than increasing or decreasing mold temperature by the same amount in 2-p as well as 1-p flows.

Now we see the effect of inlet temperature on powder segregation. Here we shall take the example of inlet temperature 500 K, 505 K and 510 K at a mold wall temperature 343 K only. As in earlier, here also we define a function "*Binder volume fraction divided by Binder plus Powder volume fraction*" and we call it "*Relative binder volume fraction*". We have taken distribution of the above function on Plane D at a mold wall temperature 343 K as shown in Fig. 5. From the Fig. 6 we shall notice that as the inlet temperature increases the value of the above function decreases that is segregation increases. Also segregation is maximum near wall region.This conforms with literature [11]. This can be traced to decreased binder viscosity with increased temperature. Looking back at Eq. (15) the drag force on particle decreases and powder segregates due to large density difference. The 2-p flow model successfully predicts this phenomenon. Segregation will increase with increasing temperature and that is why there is a limit on maximum injection temperature. In practice optimum injection temperature is found by experiment, thereby less pressure will be needed to fill the mold with minimum segregation.

In PIM process, as the powder and binder flows inside the mold, it loses its heat and if temperature falls below the liquidus temperature that is upper crystallization temperature of the binder, the solidification of the binder starts, thereby solidification of the whole mixture starts. Generally, in PIM we want to avoid this solidification process during mold filling because if solidification starts, higher injection pressure will be required to push the material or in the worst case if whole mixture solidifies, we

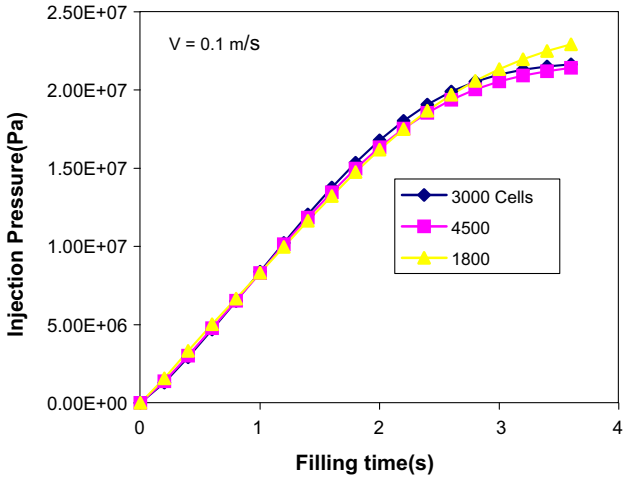

Fig. 4. Effect of grid size on injection pressure development.

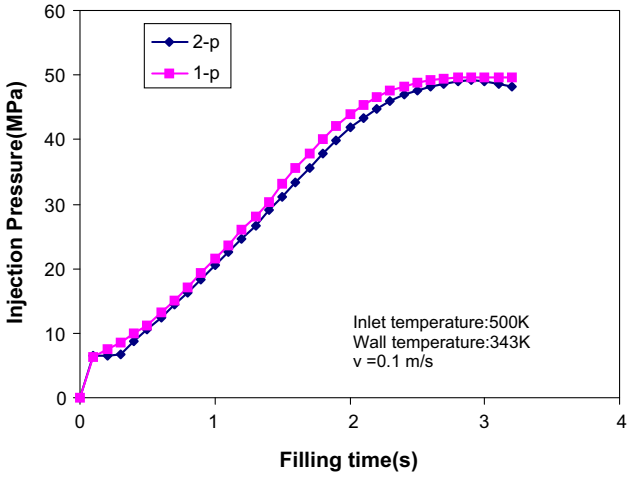

Fig. 5. Comparison of injection pressure at inlet for single-phase and multiphase model.

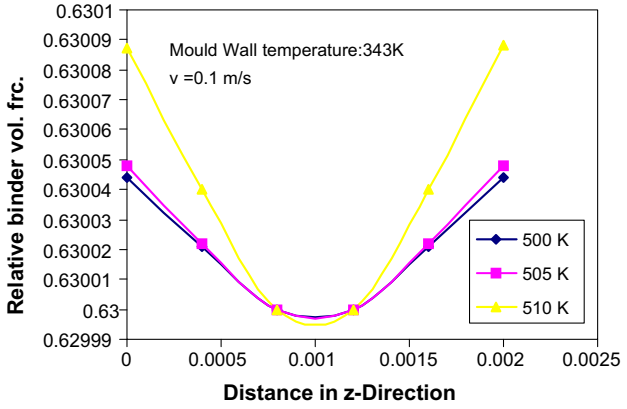

Fig. 6. Relative binder volume fraction distribution on plane A at inlet velocity 0.1 m/s, different inlet temperatures 500 K, 505 K, 510 K at the end of mould filling time 3.2 s.

cannot fill the mold at all. To avoid this PIM mold filling is generally done at sufficiently higher temperature than the liquidus temperature of the binder. And then it is allowed to solidify inside the mold after filling. The filling process in PIM is few seconds whereas the whole mold filling cycle, that is, filling and solidification will vary from approximately from 5 to 60 s [24]. Compared to mold filling time, post-filling solidification consumes more time thus in the complete injection cycle, major time is spent in post-filling solidification stage. When temperature comes below the solidus temperature that is below the lower crystallization temperature, fraction of liquid becomes zero which indicates that solidification is completed. In the following results we will show how fraction of liquid changes with temperature and time and compare the results with 1-p flow.

To illustrate the results we shall take one example at an inlet temperature of 500 K, mold wall temperature of 343 K and inlet velocity of 0.1 m/s. Since solidification is measured by amount of liquid fraction present inside the mold, to show the phenomenon we have taken the plot of liquid fraction and temperature on the centre line along the length of the mold as this is the line where material will solidify at the end and we will get the actual solidification time. As we see that just at the end of filling time 3.2 s fraction of liquid is 1.0 as Fig. 7 shows that minimum temperature is above liquidus temperature and hence solidification process does not start. Now as the time increases to 6.03 s, we notice from the Fig. 8 that liquid fraction becomes less than 1.0 as the temperature falls under liquidus temperature as seen from Fig. 9. From Fig. 10, as expected from the proposed mathematical model, liquid fraction and the temperature follow a straight line and similar trend.

The temperature distribution at the end of solidification on the center line along the length of the mold is shown in Fig. 11. It was observed that total solidification time from multiphase computation was 14.22 s as compared to 12.54 s for the single phase case. That is, the difference

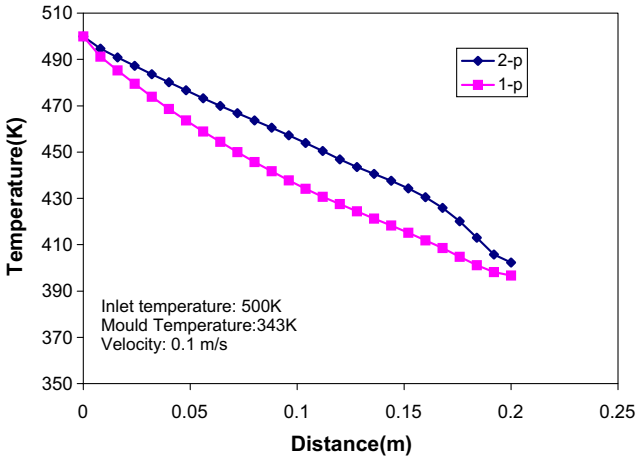

Fig. 7. Temperature distribution for 2-p and 1-p computation along a line passes through the longitudinal mid plane at time $t = 3.2$ s (at the end of mould filling).

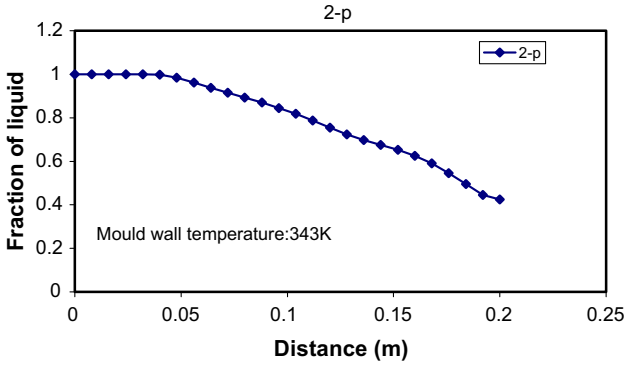

Fig. 8. Variation of liquid fraction of binder in 2-p and mixture in 1-p flow on centre line along the length of the mould at $t = 6.03$ s during solidification.

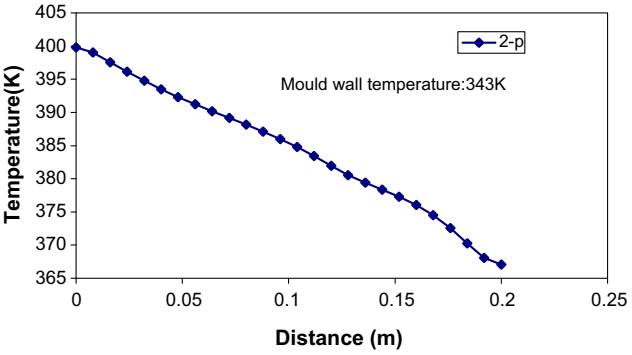

Fig. 9. Variation of temperature in 2-p and 1-p flow on center line along the length of the mould at $t = 6.03$ s during solidification.

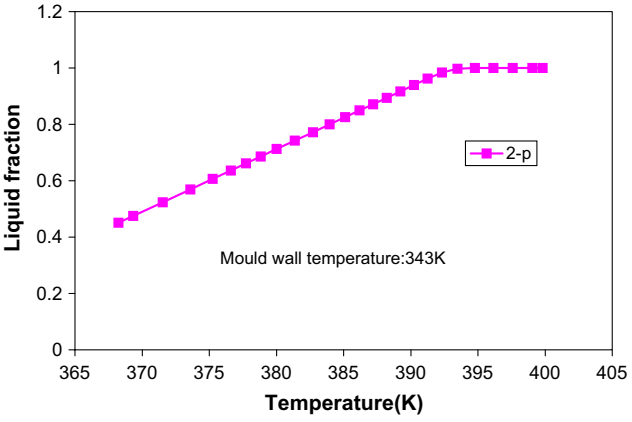

Fig. 10. Variation of temperature v/s liquid fraction of binder in 2-p flow and mixture of 1-p flow on centre line along the length of the mould at $t = 6.03$ s during solidification.

between the aforesaid solidification time is 1.68 sec and thus multiphase models predicts about 15% higher solidification time. Fig. 12 compares how temperature varies with time as the mold is filling and solidifying. It is to be seen that 2-p and 1-p temperature curves in Fig. 12 is very similar. Now we address why 2-p flow takes more time to solidify. During mold-filling, the temperature predicted from the 2-p model was higher. Now, in one hand due to

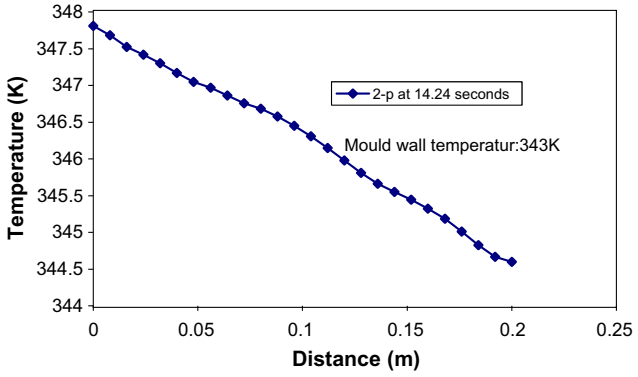

Fig. 11. Variation of temperature on the center line along the length of the mould at the end of solidification.

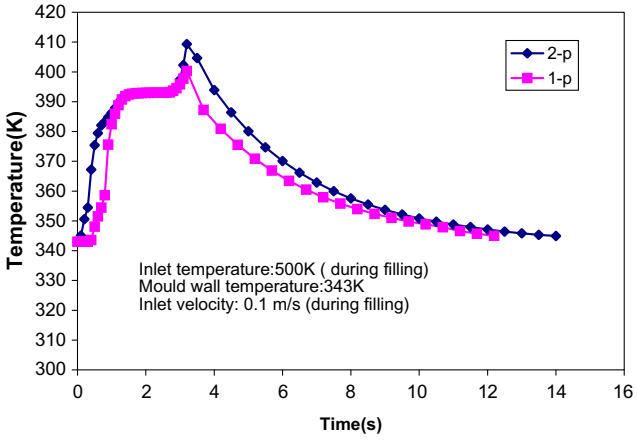

Fig. 12. Variation of temperature v/s time at a point on center line along longitudinal mid plane at a distance 0.196 m from inlet during filling till end of solidification in 2-p and 1-p flow.

this initial temperature difference, 2-p flow takes more time to come to solidification temperature. On the other hand, as we have shown earlier that along the length of the mold phase segregation occurs and due to that in the peripheral region overall thermal conductivity falls in 2-p flow whereas there is no change in 1-p thermal conductivity. There is migration of binder towards the wall leading to lower thermal conductivity, which in turn reduces the heat transfer. After the filling of mold, the conductive regime of heat transfer takes over the convective part as relatively insignificant velocity field is present inside the mold which is fast reducing to zero as solidification progresses. So mainly heat is spreading from inlet side to outlet side by conduction. Since conductivity is getting reduced towards the outlet region, rate of heat transfer is also reduced and thereby solidification process takes more time than 1-p flow.

5. Concluding remarks

An Eularian multiphase flow model has been developed for prediction of mold filling and post-filling solidification in PIM processes. The phase change of the binder is calculated through an iterative procedure balancing the latent heat. Simulation using multiphase approach could provide an insight in to the particle segregation. The temperature field could truly be predicted only in muli-phase models since effect of phase segregation is taken into account unlike the existing models.

Acknowledgements

The first author (SKS) acknowledges the financial support of DAAD for sponsoring his research stay in Foundry Institute, Aachen, Germany and also would like to acknowledge with thanks the technical support provided by the members of Numerical Simulation Group in Foundry Institute, Aachen and Foundry Group in CMERI, Durgapur, India to carry out this research work. SKS and HC gratefully acknowledge the support and encouragement received from Dr. G.P. Sinha, Director, CMERI. We thank the reviewers who have taken a lot of pain to check the manuscript and suggested improvements.

References

[1] J. Janardhana Reddy, N. Ravi, M. Vijayakumar, A simple model for viscosity of powder injection moulding mixes with binder content above powder critical binder volume concentration, J. Eur. Ceram. Soc. 20 (12) (2000) 2183–2190.
[2] Z.Y. Liu, N.H. Loh, S.B. Tor, K.A. Khor, Characterization of powder injection molding feedstock, Mater. Character. 49 (4) (2002) 313–320.
[3] B. Huang, S. Liang, X. Qu, The rheology of metal injection molding, J. Mater. Process. Technol. 137 (1-3) (2003) 132–137.
[4] L.A. Najami, D. Lee, Modelling of the mould filling process for powder injection moulding, Polym. Eng. Sci. 31 (15) (1991) 1137.
[5] L.A. Najmi, D. Lee, Application of the mould filling simulation to powder injection moulding, Int. J. Powder Metall. 30 (2) (1994) 231–240.
[6] C.W. Wang, A finite-difference computing model for 3-D simulation of the powder injection process, in: Powder Injection Moulding Symposium 1992, pp. 435–449.
[7] B. Lanteri, H. Burlet, A. Poitou, I. Campion, Powder injection moulding, an original simulation of paste flow, Eur. J. Mechan. A/Solids 15 (3) (1996) 465–485.
[8] T.H. Kwon, J.B. Park, Finite element analysis modelling of powder injection mould filling process including yield stress and slip phenomenon, Polym. Eng. Sci. 35 (9) (1995) 741–753.
[9] V.V. Bilovol, L. Kowalski, J. Duszczyk, Numerical simulation of the powder injection moulding process for optimization of mould design and process parameters, Adv. Eng. Mater. 2 (3) (2000) 127–131.
[10] F. Ilinca, J.-F. Hetu, A. Derdouri, Metal injection moulding, 3D modelling of non isothermal filling, Polym. Eng. Sci. 42 (4) (2002) 760–770.
[11] Y.C. Lam, X. Chen, K.C. Tam, S.C.M. Yu, Simulation of particle migration of powder-resin system in injection moulding, Trans. ASME 125 (2003) 538–547.
[12] T. Brrière, J.C. Gelin, B. Liu, Experimental and numerical investigations on properties and quality of parts produced by MIM, Powder Metall. 44 (3) (2001) 228–234.
[13] T. Barrière, J.C. Gelin, B. Liu, Determination of the optimal processparameters in metal injection moulding from experiments and numerical modeling, J. Mater. Process. Technol. 143-144 (2003) 636–644.

[14] T. Barrière, J.C. Gelin, B. Liu, Improving mould design and injection parameters in metal injection moulding by accurate 3D finite element simulation, J. Mater. Process. Technol. 125–126 (9) (2002).
[15] M. Ishii, N. Zuber, Drag coefficient and relative viscosity in bubbly, droplet or particulate flow, AIChE J. 25 (1979) 843–855.
[16] Y. Wang, S. Ahuja, C. Beckerman, H.C. de GROH III, Multiparticle interfacial drag in equiaxed solidification, Metall. Mater. Trans. B 26B (1995) 111–119.
[17] L. Schiller, Z. Naumann, Z. Ver. Deutsch. Ing. 77 (318) (1935).
[18] W.E. Ranz, W.R. Marshal Jr., Evaporation from drops part I, Chem. Eng. Prog. 48 (3) (1952) 141–146.
[19] D.J. Gun, Transfer of heat and mass to particles in fixed and fluidised beds, Int. J. Heat Mass Transfer 21 (1978) 467–476.
[20] R.L. Goff, G. Poutot, D. Delaunay, R. Fulchiron, E. Koscher, study and modeling of heat transfer during solidification of semi-crystalline polymers, Int. J. Heat Mass Transfer 48 (2005) 5417–5430.
[21] FLUENT Users' Guide 6.2, Fluent Inc., Lebanon,USA,2005.
[22] S.K. Samanta, Mathematical modeling and simulation of Powder Injection Mould filling and solidification, Report of Foundry Institute Aachen, September 2005.
[23] A. Kumar, P.S. Ghoshdastidar, M.K. Muju, Computer simulation of transport processes during injection mould filling and optimization of the moulding conditions, J. Mater. Process. Technol. 120 (2002) 438–449.
[24] R.M. German, Powder Injection Moulding, Renssler Polytechnique Institute, New York, 1990.